ISSN 1070-3284, Russian Journal of Coordination Chemistry, 2023, Vol. 49, No. 5, pp. 276–285. © Pleiades Publishing, Ltd., 2023.
Russian Text © The Author(s), 2023, published in Koordinatsionnaya Khimiya, 2023, Vol. 49, No. 5, pp. 278–289.

Heteroleptic Metal-Organic Frameworks of Lanthanides (La, Ce, and Ho) Based on Ligands of the Anilate Type and Dicarboxylic Acids

O. Yu. Trofimova[a], A. V. Maleeva[a], K. V. Arsen'eva[a], A. V. Klimashevskaya[a], A. V. Cherkasov[a], and A. V. Piskunov[a, *]

[a] *Razuvaev Institute of Organometallic Chemistry, Russian Academy of Sciences, Nizhny Novgorod, Russia*
**e-mail: pial@iomc.ras.ru*

Received October 24, 2022; revised November 9, 2022; accepted November 9, 2022

Abstract—New heteroleptic metal-organic frameworks of lanthanides, units of which contain anionic organic ligands of two types, are prepared by the solvothermal synthesis in *N*,*N*-dimethylformamide (DMF). The cross-linked coordination polymer $[Ho_2(CA)_2(Bdc)\cdot 4DMF]$ (**I**) and two scaffold derivatives $[La_2(pQ)_2(Bpdc)\cdot 4DMF]$ (**II**) and $[Ce_2(CA)(Bdc)_2\cdot 4DMF]\cdot 2DMF$ (**III**·2DMF), where CA is chloranilic acid dianion, pQ is 2,5-dihydroxy-3,6-di-*tert*-butyl-*para*-benzoquinone dianion, Bdc is terephthalic acid dianion, and Bpdc is 4,4'-biphenyldicarboxylic acid dianion, are synthesized. The structures of compounds **I**, **II**, and **III**·2DMF are studied by X-ray diffraction (XRD) (CIF file CCDC nos. 2212230, 2212231, and 2212232, respectively).

Keywords: anilate ligand, metal-organic frameworks, dicarboxylic acids, redox-active ligand, XRD, solvothermal synthesis

DOI: 10.1134/S1070328423600183

INTRODUCTION

Metal-organic frameworks (MOFs) represent a special class of microporous and mesoporous solid substances that have actively been studied for two recent decades [1–4]. Researchers are highly interested in these derivatives due to prospects of their wide application as diverse functional materials [5–9]. In particular, MOFs and related composites can be used as sorbents [10–13]; heterogeneous catalysts [14]; luminescent [15, 16], electrochemical, or physical sensors [17, 18]; and electroconducting [19–21] and magnetic materials [22, 23]. The crystal structure, topology, and physical and chemical properties of MOFs depend on the nature of metal ions and organic ligands involved in their formation. A unique trend of the development of the MOF chemistry is the preparation and study of the properties of the compounds containing ligands of different types in one derivative. A combination of anionic ligands of different types in the MOF unit makes it possible to synthesize structures of new types with a set of properties due to which they favorably differ from the homoleptic derivatives [24–30].

In this work, we present the synthesis and results of studying the structural diversity of new lanthanide MOFs: $[Ho_2(CA)_2(Bdc)\cdot 4DMF]$ (**I**), $[La_2(pQ)_2(Bpdc)\cdot 4DMF]$ (**II**), and $[Ce_2(CA)(Bdc)_2\cdot 4DMF]\cdot 2DMF$ (**III**·2DMF), where CA is chloranilic acid dianion, pQ is 2,5-dihydroxy-3,6-di-*tert*-butyl-*para*-benzoquinone dianion, Bdc is terephthalic acid dianion, Bpdc is 4,4'-biphenyldicarboxylic acid dianion, and DMF is *N*,*N*-dimethylformamide. It should be mentioned that 2,5-dihydroxy-3,6-di-*tert*-butyl-*para*-benzoquinone has been used not long ago for MOF formation and, therefore, only several MOFs based on this compound are known [25, 30–32].

EXPERIMENTAL

IR spectra were recorded on an FSM-1201 FT-IR spectrometer (suspensions in Nujol, KBr pellets). Elemental analysis was carried out on an Elementar Vario El cube instrument. Compound **III** was studied by thermogravimetry on a Mettler Toledo TGA/DSC3+ instrument at 30–700°C under a nitrogen atmosphere (crucible of polycrystalline alumina) at a heating rate of 5°C/min. The following commercial reagents were used: DMF, $LaCl_3\cdot 7H_2O$, $Ce(NO_3)_3\cdot 6H_2O$, $HoCl_3\cdot 6H_2O$, chloranilic acid (H_2CA), terephthalic acid (H_2Bdc), and 4,4'-biphenyldicarboxylic acid (H_2Bpdc). 2,5-Dihydroxy-3,6-di-*tert*-butyl-*para*-benzoquinone (H_2pQ) was synthesized according to a known procedure [33].

Synthesis of $[Ho_2(CA)_2(Bdc)\cdot 4DMF]$ (I), $[La_2(pQ)_2(Bpdc)\cdot 4DMF]$ (II), and $[Ce_2(CA)(Bdc)_2\cdot 4DMF]\cdot 2DMF$ (III·2DMF). A mixture of a lanthanide salt ($HoCl_3\cdot 6H_2O$ for MOF **I**, $LaCl_3\cdot 7H_2O$ for MOF **II**, and $Ce(NO_3)_3\cdot 6H_2O$ for MOF **III**), dicar-

boxylic acid (H_2Bdc for MOFs **I** and **III**, H_2Bpdc for MOF **II**) and 3,6-substituted anilic acid (H_2CA for MOFs **I** and **III**, H_2pQ for MOF **II**) was triturated in a mortar for better mixing of the starting components. The obtained mixture in DMF (5 mL) was heated at 80°C in a sealed glass tube for 3 days, the temperature was increased to 130°C, and the mixture was heated at this temperature for 24 h.

MOFs **I** and **II** were obtained as crystalline products colored in brown and violet, respectively. The synthetic systems also exhibit by-products: crystalline colorless lanthanide carboxylates. The variation of the ratio of the starting components and reaction conditions did not allowed us to synthesize phase-pure products.

MOF **III**·2DMF was synthesized at the starting component ratio $Ce(NO_3)_3 \cdot 6H_2O$: H_2bdc : H_2CA = 1 : 2 : 1 as fine brown orthorhombic crystals, which were collected on the Schott filter and washed with DMF (3 mL). The yield was 60%. According to the XRD data, the synthesized scaffold polymer contains two molecules of the "guest" solvent (DMF) per MOF unit. On drying in air, compound **III** lost crystallinity because of the displacement of the "guest" solvent from the pores. According to the elemental analysis data, dried MOF **III** contained no "guest" solvent.

For $C_{34}H_{36}N_4O_{16}Cl_2Ce_2$			
Anal. calcd., %	C, 36.86	H, 3.28	N, 5.06
Found, %	C, 36.63	H, 3.48	N, 5.15

IR (ν, cm^{-1}): 1673 s, 1651 s, 1605 s, 1588 s, 1518 s, 1312 m, 1294 m, 1256 m, 1155 m, 1107 m, 1065 w, 1030 w, 1015 w, 995 w, 889 m, 862 w, 839 s, 787 w, 754 s, 675 s, 640 m, 594 m, 576 m, 511 s.

XRD of MOFs **I**, **II**, and **III**·2DMF was carried out on Bruker D8 Quest (**I**, **III**) and Rigaku OD Xcalibur *E* (**II**) diffractometers (MoK_α radiation, ω scan mode, λ = 0.71073 Å) at T = 100.0(2) K. Experimental sets of intensities were measured and integrated, an absorption correction was applied, and the structures were solved and refined using the APEX3 [34], CrysAlis^{Pro} [35], SADABS [36], and SHELX [37] software. The structures were solved using the dual-space algorithm [38] and refined by full-matrix least squares for F^2_{hkl} in the anisotropic approximation for non-hydrogen atoms. Hydrogen atoms of MOFs **I**–**III** were placed in the geometrically calculated positions and refined isotropically with fixed thermal parameters $U_{iso}(H) = 1.2U_{eq}(C)$ ($U_{iso}(H) = 1.5U_{eq}(C)$ for methyl groups). The crystallographic data and experimental XRD parameters for MOFs **I**–**III** are given in Table 1. Selected bond lengths are listed in Table 2.

The structures were deposited with Cambridge Crystallographic Data Centre (CIF files CCDC nos. 2212230 (**I**), 2212231 (**II**), and 2212232 (**III**·2DMF) and are available at ccdc.cam.ac.uk/structures).

RESULTS AND DISCUSSION

Heteroleptic lanthanide (La, Ce, and Ho) MOFs were prepared by the two-stage solvothermal synthesis (Scheme 1). The reaction occurs in a sealed glass tube. At the first stage, the reaction mixture was heated to 80°C for 3 days. At the second stage, the thermostat temperature was increased to 130°C, and the reaction mixture was heated for 24 h more. The reaction affords crystalline heteroligand MOFs. Compound $[Ce_2(CA)(Bdc)_2 \cdot 4DMF] \cdot 2DMF$ (**III**·2DMF) was isolated as a finely crystalline brown product. The purity of the synthesized derivative was confirmed by elemental analysis and IR spectroscopy data. The thermal stability was studied by thermogravimetry (TG). Derivatives **I** and **II** are crystalline products, but the presence of several components in the initial mixtures does not allow one to achieve the phase purity of the synthesized samples. Variations of the synthesis conditions and ratios of the starting reagents do not result in substantial changes in the purity of the desired products, unlike derivative **III**·2DMF and previously described lanthanum 3D MOFs [25]. The structures of synthesized MOFs **I**, **II**, and **III**·2DMF were studied by single-crystal XRD.

The molecular and crystal structures of MOFs **I**, **II**, and **III**·2DMF were determined by XRD. The molecular structures of compounds **I**–**III** are shown in Figs. 1–3. In spite of using components of the same type in the synthesis of the heteroleptic derivatives, the synthesized compounds structurally differ substantially from each other. The formation of these or other products is affected by such factors as the ionic radius of lanthanides [39] and different types of coordination of the anilate [40–42] (Scheme 2) and dicarboxylate ligands (Scheme 3) [43] to the metal atom.

According to the XRD data, derivative **I** crystallizes in the monoclinic symmetry group $P2_1/c$ and is a 2D polymer with the network topology **sql** [44–46]. MOFs **II** and **III** crystallize in the space groups $P2_1/c$ and $P\bar{1}$, respectively, and form scaffold polymers with the topologies **mog** (La) and **xah** (Ce) [44–46].

The repeated units of MOFs **I** and **II** contain two lanthanide atoms linked by the C(O)O bridges of two dicarboxylate ligands (Figs. 1, 2; Scheme 1). The eight-coordinate environment of each Ln atom is formed by four oxygens of two anilate ligands, two oxygens of the bridging carboxylate groups of two dicarboxylic acids, and two oxygens of the coordinated DMF molecules (Figs. 1 and 2).

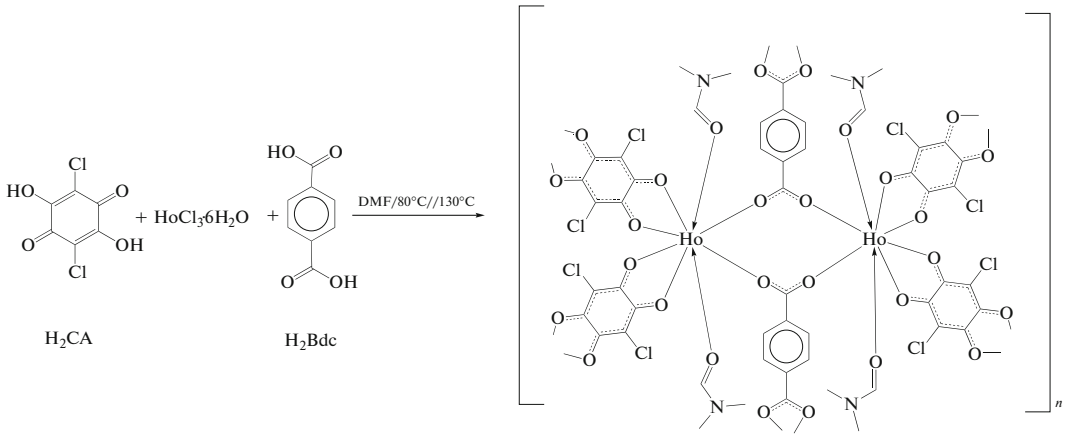

$[Ho_2(CA)_2(Bdc)\cdot 4DMF]$ (**I**)

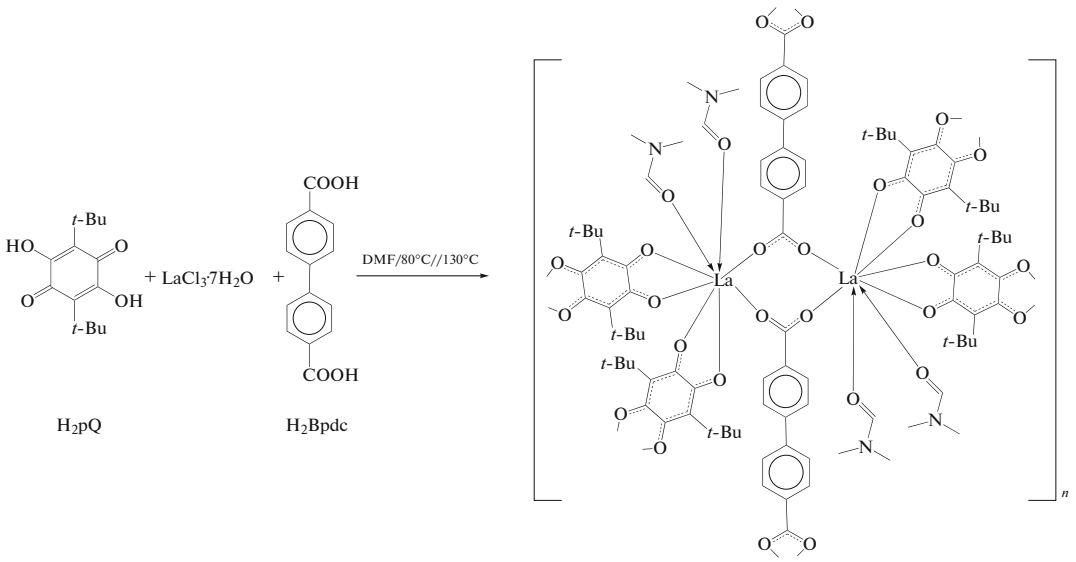

$[La_2(pQ)_2(Bpdc)\cdot 4DMF]_n$ (**II**)

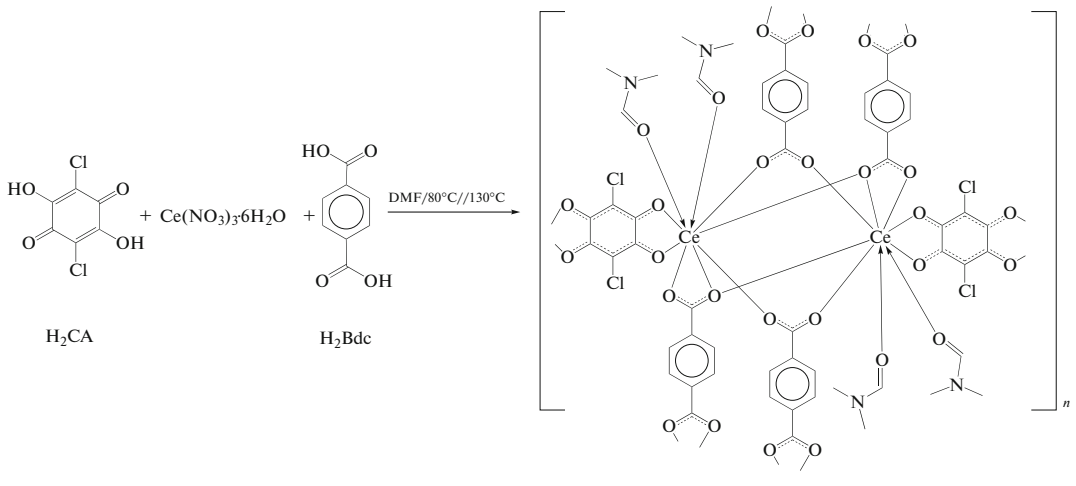

$[Ce_2(CA)(Bdc)_2\cdot 4DMF]$ (**III**)

Scheme 1.

Table 1. Crystallographic data and experimental and structure refinement parameters for compounds **I**, **II**, and **III**·2DMF

Parameters	Value		
	I	**II**	**III**·2DMF
Empirical formula	$C_{32}H_{32}N_4O_{16}Cl_4Ho_2$	$C_{54}H_{72}N_4O_{16}La_2$	$C_{40}H_{50}N_6O_{18}Cl_2Ce_2$
Crystal sizes, mm	0.08 × 0.04 × 0.03	0.30 × 0.14 × 0.10	0.12 × 0.11 × 0.06
Crystal system	Monoclinic	Monoclinic	Triclinic
Space group	$P2_1/c$	$P2_1/c$	$P\bar{1}$
a, Å	13.3895(7)	12.4328(6)	10.5710(4)
b, Å	16.3007(8)	19.6854(10)	10.9919(4)
c, Å	10.0578(5)	12.3921(5)	12.4078(4)
α, deg	90	90	115.0480(10)
β, deg	112.044(2)	109.522(5)	99.6880(10)
γ, deg	90	90	105.1540(10)
V, Å^3	2034.72(18)	2858.5(3)	1194.85(7)
Z	2	2	1
ρ_{calc}, g/cm^3	1.959	1.523	1.743
μ, mm^{-1}	4.197	1.544	2.071
θ_{min}–θ_{max}, deg	2.06–25.12	2.88–26.02	2.20–27.15
Number of observed reflections	24889	17252	12014
Number of independent reflections ($I > 2\sigma(I)$)	3028	4096	4760
R_{int}	0.0998	0.0504	0.0280
$S(F^2)$	1.038	1.008	1.059
R_1/wR_2 ($F^2 > 2\sigma(F^2)$)	0.0516/0.0874	0.0402/0.0818	0.0253/0.0539
R_1/wR_2 (for all parameters)	0.0747/0.0948	0.0691/0.0919	0.0307/0.0558
$\Delta\rho_{max}/\Delta\rho_{min}$, e/Å^3	1.76/–2.16	1.19/–0.73	0.90/–0.94

It was found by an analysis of the coordination environment of the lanthanide atoms in MOFs **I** and **II** by the Shape 2.1 program [47, 48] that the optimum approximation parameters corresponded to the structures of a tetragonal antiprism (SAPR-8, CShM = 1.168) and a trigonal dodecahedron (TDD-8, CShM = 1.579) for MOFs **I** and **II**, respectively (Fig. 4).

The lanthanum MOFs related to compound **II** and based on the anilate and dicarboxylate ligands [25] were characterized by nine-coordinate metal centers and a different ratio of the bridging organic dianions (anilate : dicarboxylate = 2 : 1 (**I** and **II**) and 1 : 2 in [25]). According to this ratio, compounds **I** and **II** are identical to the recently published heteroleptic MOFs of erbium [24] and ytterbium [26]. The distance between two Ho atoms linked to the carboxylate group in MOF **I** is 5.39 Å, which is substantially shorter than the corresponding La...La distance in compound **II** (5.83 Å), and is well consistent with a change in the ionic radii of the corresponding elements. A substantial distinction of the structures of units of MOFs **I** and **II** is the arrangement of the coordinated solvent molecules. The angle between the coordinated DMF molecules O(7)Ho(1)O(8) in MOF **I** is 151.4(2)°, and the O(7)La(1)O(8) angle in MOF **II** is 73.0(2)°. Thus, the relative arrangement of DMF molecules in the MOF unit is mutually related to the topology of the whole structure formed. For instance, the holmium derivative, as its analogs based on Er [24] and Yb [26], forms 2D polymer networks, whereas the units of the lanthanum compounds form a cage (Fig. 5).

The unit of MOF **III**·2DMF also consists of two Ce(III) centers (Fig. 3). However, the cerium atoms are linked to each other by the bridging –C(O)O fragments of four dicarboxylate ligands (Scheme 1). Each Ce(III) center coordinates five oxygen atoms of four Bdc^{2-} anions, two oxygen atoms of the CA^{2-} anions, and oxygen atoms of two coordinated DMF molecules (Fig. 3).

Thus, the ratio of the anionic bridging ligands in MOF **III**·2DMF is anilate : dicarboxylate = 1 : 2, and the formal coordination number of the cerium atom is nine. The formation of units of this type in the heteroligand systems was demonstrated earlier for the lanthanum derivatives containing dianions of terephthalic and anilic acids [25]. The distance between the Ce(III) atoms linked by the bridging carboxylate groups in the unit of MOF **III**·2DMF is 4.26 Å. The angle between the coordinated DMF molecules O(7)Ce(1)O(8) in MOF **III** is 74.40(6)°. An analysis of the coordination polyhedron in compound

Table 2. Selected bond lengths (Å) in compounds **I**, **II**, and **III**·2DMF*

I		**II**		**III**·2DMF	
Bond	*d*, Å	Bond	*d*, Å	Bond	*d*, Å
Ho(1)–O(1)	2.436(7)	La(1)–O(1)	2.523(3)	Ce(1)–O(1)	2.542(2)
Ho(1)–O(2)	2.388(8)	La(1)–O(2)	2.447(3)	Ce(1)–O(2A)	2.556(2)
Ho(1)–O(3)	2.372(7)	La(1)–O(3D)	2.547(3)	Ce(1)–O(3)	2.464(2)
Ho(1)–O(4)	2.416(7)	La(1)–O(4D)	2.506(3)	Ce(1)–O(4B)	2.473(2)
Ho(1)–O(5)	2.21(2)	La(1)–O(5)	2.438(3)	Ce(1)–O(5)	2.442(2)
Ho(1)–O(6C)	2.30(2)	La(1)–O(6C)	2.425(3)	Ce(1)–O(5B)	2.860(2)
Ho(1)–O(7)	2.348(5)	La(1)–O(7)	2.535(3)	Ce(1)–O(6B)	2.488(2)
Ho(1)–O(8)	2.375(6)	La(1)–O(8)	2.526(4)	Ce(1)–O(7)	2.495(2)
O(1)–C(1)	1.27(2)	O(1)–C(1)	1.265(5)	Ce(1)–O(8)	2.544(2)
O(2)–C(2)	1.27(2)	O(2)–C(2)	1.258(5)	O(1)–C(1)	1.259(3)
C(1)–C(2)	1.51(2)	O(3)–C(4)	1.260(5)	O(2)–C(3)	1.247(3)
C(2)–C(3)	1.39(2)	O(4)–C(5)	1.271(5)	C(1)–C(2)	1.394(4)
C(1)–C(3A)	1.38(2)	C(1)–C(2)	1.561(6)	C(2)–C(3)	1.414(4)
O(3)–C(4)	1.26(2)	C(2)–C(3)	1.388(6)	C(1)–C(3A)	1.535(4)
O(4)–C(5)	1.28(2)	C(3)–C(4)	1.410(6)	O(3)–C(4)	1.257(3)
C(4)–C(5)	1.54(2)	C(4)–C(5)	1.560(6)	O(4)–C(4)	1.264(3)
C(5)–C(6)	1.35(2)	C(5)–C(6)	1.399(6)	C(4)–C(5)	1.508(3)
C(4)–C(6B)	1.40(2)	C(1)–C(6)	1.405(6)	C(5)–C(6)	1.392(4)
O(5)–C(7)	1.26(2)	O(5)–C(15)	1.249(5)	C(6)–C(7)	1.386(4)
O(6)–C(7)	1.25(2)	O(6)–C(15)	1.258(5)	C(5)–C(7C)	1.393(4)
C(7)–C(8)	1.49(2)	C(15)–C(16)	1.505(5)	O(5)–C(8)	1.272(3)
C(8)–C(9)	1.36(2)	C(16)–C(17)	1.350(7)	O(6)–C(8)	1.253(3)
C(8)–C(10)	1.43(3)	C(17)–C(18)	1.396(7)	C(8)–C(9)	1.498(4)
C(9)–C(10D)	1.39(2)	C(18)–C(19)	1.359(7)	C(9)–C(10)	1.397(4)
		C(19)–C(20)	1.371(7)	C(10)–C(11)	1.379(4)
		C(20)–C(21)	1.382(6)	C(9)–C(11D)	1.395(4)
		C(16)–C(21)	1.382(7)		
		C(19)–C(19B)	1.504(8)		

* Symmetry transforms used for generating equivalent atoms: (A) $-x-1, -y+2, -z-1$; (B) $-x-1, -y+2, -z$; (C) $-x-2, -y+2, -z-1$; (D) $-x-2, -y+2, -z-2$ (**I**). (A) $x, -y+1/2, z-1/2$; (B) $-x+2, -y+1, -z+2$; (C) $-x+1, -y+1, -z+1$; (D) $x, -y+1/2, z+1/2$ (**II**). (A) $-x+1, -y, -z+2$; (B) $-x+1, -y, -z+1$; (C) $-x+1, -y+1, -z+1$; (D) $-x, -y, -z+1$ (**III**·2DMF).

III·2DMF by the Shape 2.1 program [47–49] allowed one to establish the maffin structure (MFF-9, CShM = 1.224) (Fig. 4).

Possible types of coordination of the dicarboxylate ligands to the metal atom are shown in Scheme 2. Anilate ligands in the dianionic form can act as both the bridging (bis)bidentate ligands (Scheme 2, types 1 and 2) and the terminal bidentate ligand with the *ortho*-quinoid structure (Scheme 2, type 3). The chloranilic acid dianions in compounds **I** and **III**·2DMF and the 2,5-dihydroxy-3,6-di-*tert*-butyl-*para*-quinone dianion in MOF **II** consist of two delocalized π-electron OCCCO systems linked by ordinary C–C bonds (Scheme 2, type 1). The range of distances for ordinary C–C bonds in the anilate dianions for MOFs **I**, **II**, and **III**·2DMF is 1.51(2)–1.561(6) Å (Table 2). Other C–C distances of the six-membered cycles range from 1.35 to 1.41 Å. The C–O interatomic distances are intermediate between those for double and ordinary oxygen–carbon bonds and lie in a narrow range of distances of 1.258(5)–1.28(2) Å.

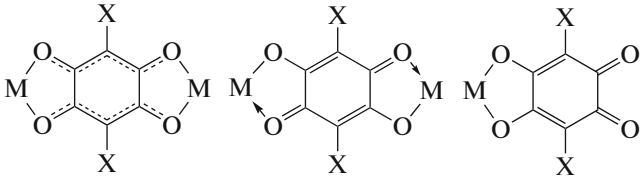

Scheme 2.

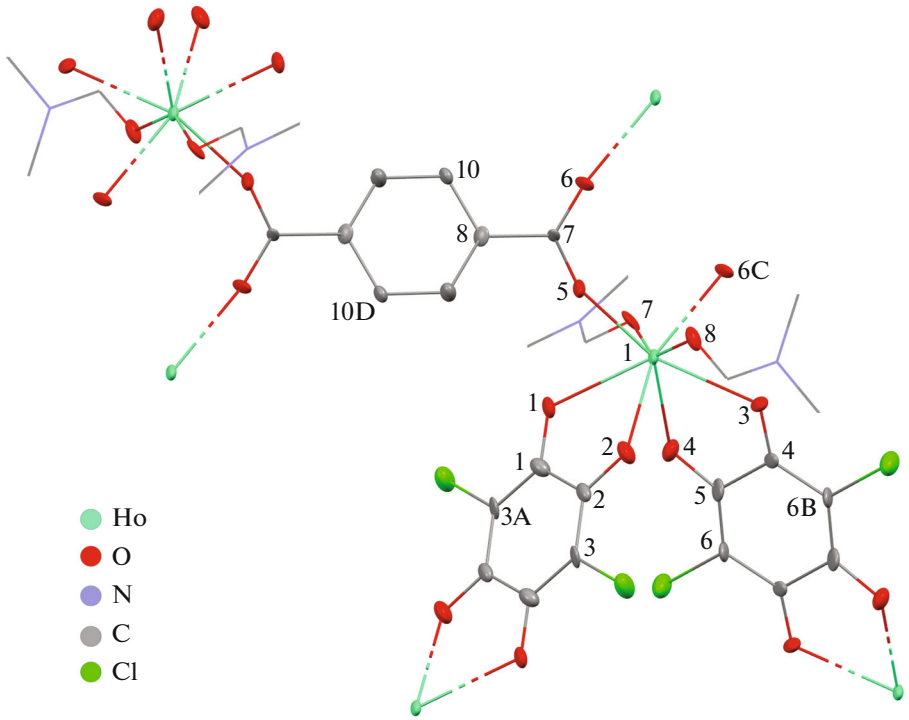

Fig. 1. Molecular structure of the unit of MOF **I**. Thermal ellipsoids are given with 50% probability. Hydrogen atoms are omitted.

In all derivatives, the dicarboxylate ligands perform the function of a bridging ligand binding four Ln^{3+} ions. Possible types of coordination of the dicarboxylate ligands to the metal atom are shown in Fig. 3. Each C(O)O group of the dicarboxylate ligand in MOF **I** and **II** (Figs. 1 and 2) coordinates via the μ_2-κ^1:κ^1 mode (Scheme 3, type 1).

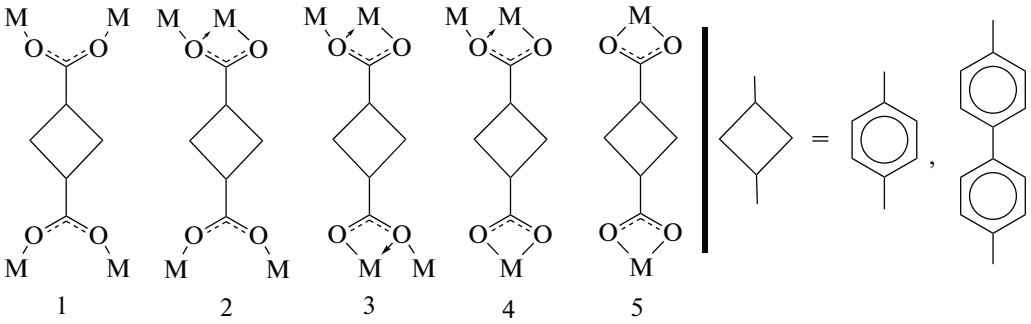

Scheme 3.

Cerium derivative **III**·2DMF for two of four dicarboxylate ligands exhibits the same coordination mode μ_2-κ^1:κ^1 for each C(O)O group (type 1 in Scheme 3) similarly to compounds **I** and **II**. However, two other ligands accomplish the coordination mode for each C(O)O group: μ_2-κ^1:κ^2 (type 3 in Scheme 3). Two coordination types of the dicarboxylate ligands in derivative **III**·2DMF are distinctly demonstrated in Fig. 6.

The formed dicarboxylate network is cross-linked into a three-dimensional cage by chloranilic acid dianions. The formed scaffold polymer of cerium contains pores accessible for the solvent molecules, whose volume is 19.8% of the crystalline unit cell volume. The pores are occupied by two "guest" DMF molecules based on two cerium ions (Fig. 7).

It should be mentioned that single-crystal samples of cerium compound **III**·2DMF rapidly decompose on storage in air, which is due to the loss of the guest solvent. This is indicated by the elemental analysis data for the samples after decomposition, which show a good convergence of the results for the compounds with the simplest formula $[Ce_2(CA)(Bdc)_2 \cdot 4DMF]$ (**III**). According to the TG analysis data, MOF **III** has

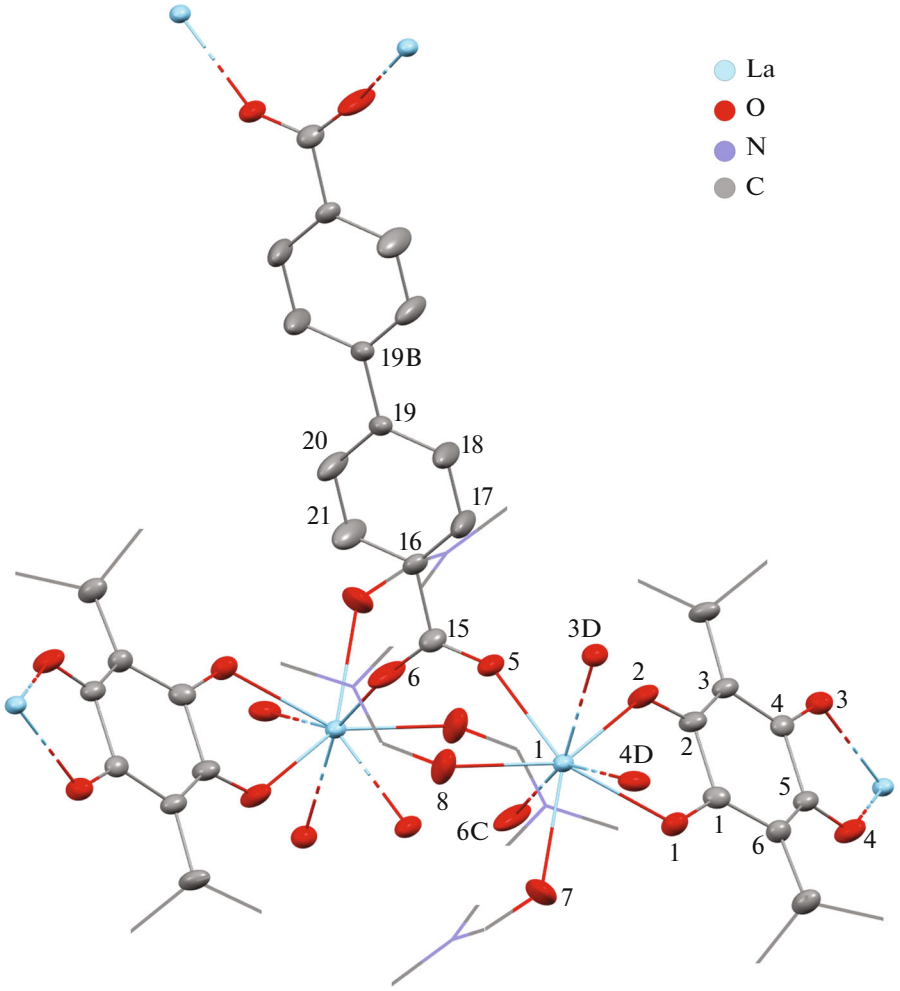

Fig. 2. Molecular structure of the unit of MOF **II**. Thermal ellipsoids are given with 50% probability. Hydrogen atoms are omitted.

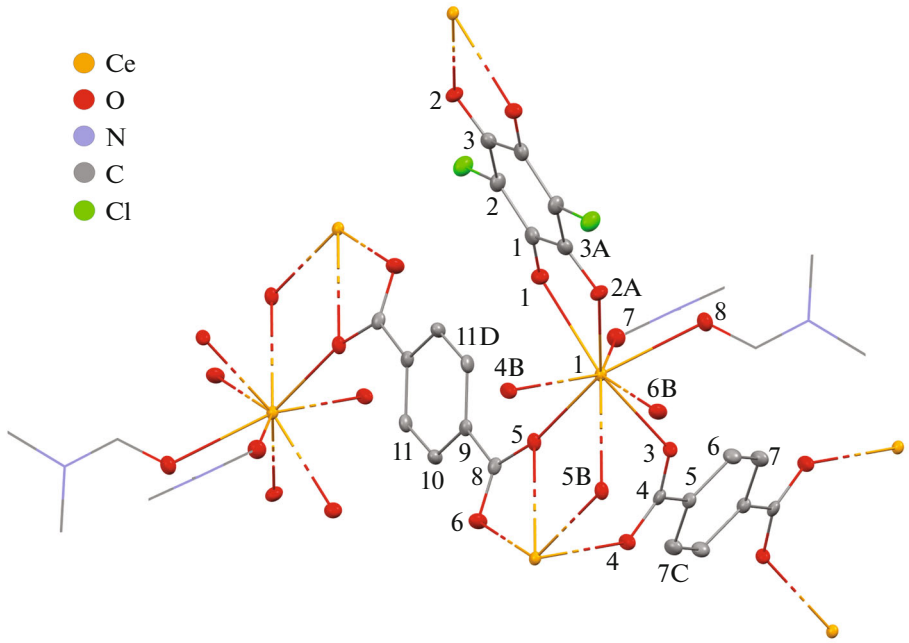

Fig. 3. Molecular structure of the unit of MOF **III**·2DMF. Thermal ellipsoids are given with 50% probability. Hydrogen atoms and "guest" DMF molecules are omitted.

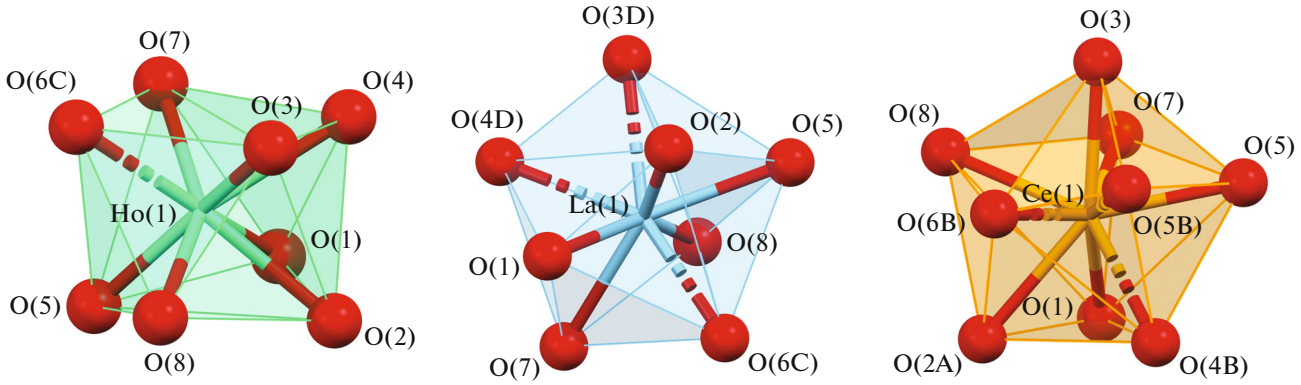

Fig. 4. Structures of the coordination polyhedra of MOFs **I**, **II**, and **III**·2DMF.

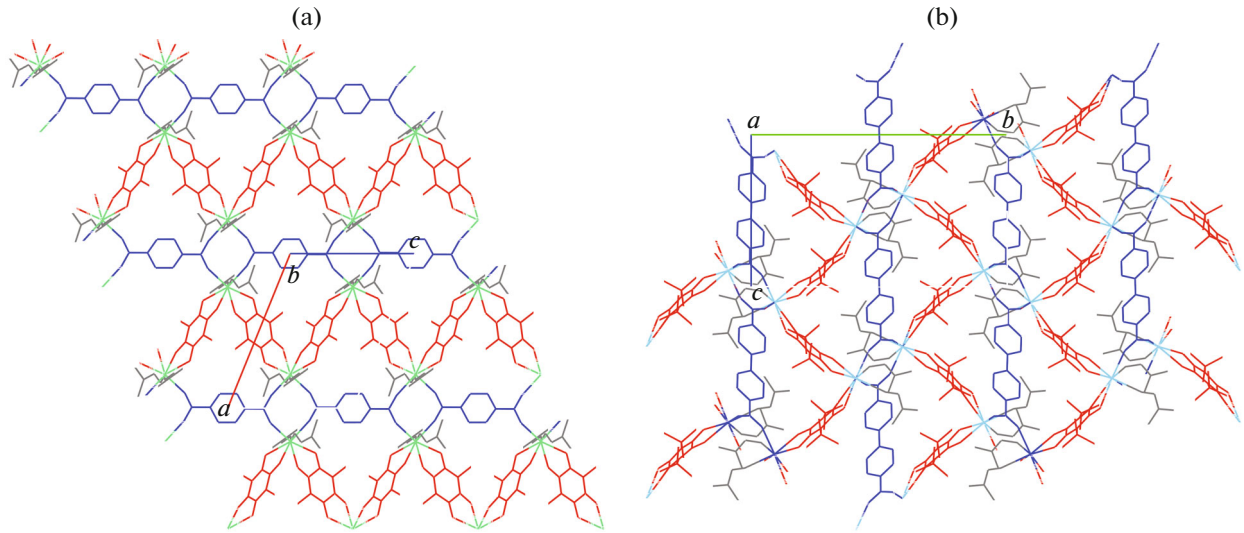

Fig. 5. (a) Network of MOF **I** along the (010) vector and (b) the cage of MOF **II** along the (100) vector. Color codes: Ho is green, La is blue, anilate ligand is red, dicarboxylate ligand is dark blue, and DMF is gray.

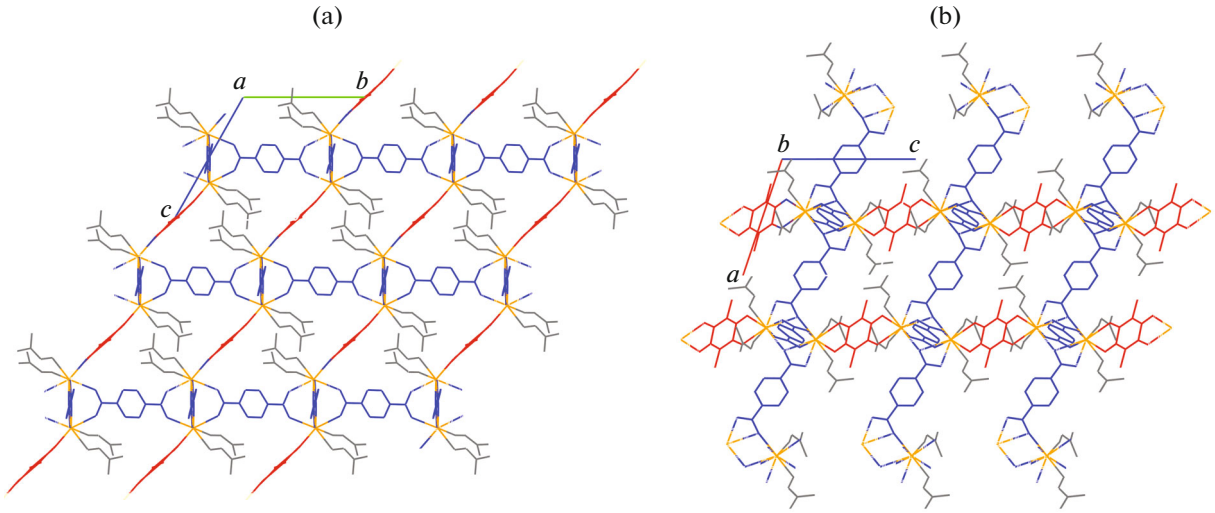

Fig. 6. Cage of MOF **III**·2DMF along the (a) (100) and (b) (010) vectors. Color codes: Ce is orange, anilate ligand is red, dicarboxylate ligand is blue, and DMF is gray. "Guest" DMF molecules are omitted.

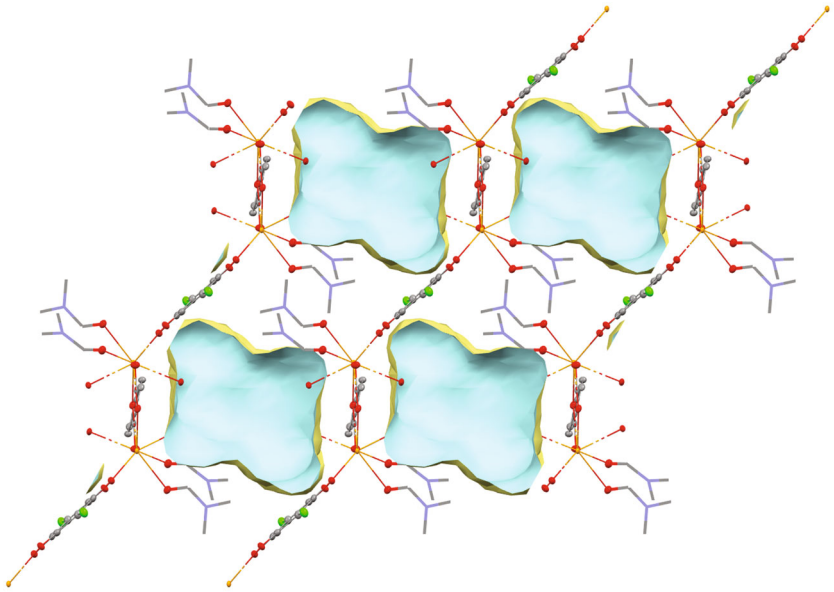

Fig. 7. Cavities in the crystal packing of MOF **III**·2DMF along the (100) vector. The pore volumes are calculated with a probe radius of 1.2 Å and an increment of 0.7 Å. The external pore surface is yellow, and the internal pore surface is blue. "Guest" DMF molecules are omitted.

no high thermal stability of the anionic cage (Fig. 8). The TG curve demonstrates a low mass loss (~3%) on heating to 150°C associated, most likely, with the removal of the residual solvent from the interstitial space. The second stage corresponds to 13% in a range of 150–250°C and is consistent with the value calculated for two molecules of coordinated DMF per formula unit of MOF. Further, the remained two DMF molecules are removed from the cerium ions in a temperature range of 260–400°C, and the mass loss on the curve for this stage is 13% as well. A subsequent increase in the temperature above 530°C results in the final decomposition of the polymer. It should be mentioned that the thermal stability of the cerium MOF substantially exceeds that for the related lanthanum derivatives [25], for which the thermal decomposition of the anionic cage starts at temperatures about 300°C.

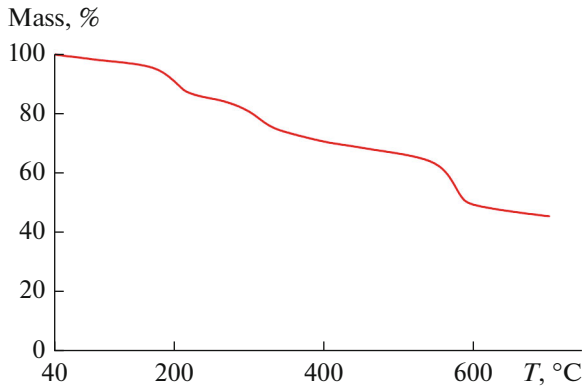

Fig. 8. TG curve for MOF **III**.

Thus, new heteroleptic metal-organic frameworks of lanthanides containing anionic ligands of two types in the unit (anilate and dicarboxylate) were synthesized. It is shown that both the metal center nature and the character of coordination of the ligands of both types affect the unit structure. The cerium MOF was isolated in the analytically pure state, which was confirmed by the elemental analysis, thermogravimetry, and IR spectroscopy data. The study showed a high stability of derivative **III**: its cage decomposes at temperatures above 530°C.

ACKNOWLEDGMENTS

The work was carried out using the equipment of the Center for Collective Use "Analytical Center of Institute of Organometallic Chemistry of Russian Academy of Sciences" and supported by the project "Provision of Development of Material Technical Infrastructure of Centers for Collective Use of Scientific Equipment" (unique identifier RF–2296.61321X0017, agreement no. 075-15-2021-670).

FUNDING

This work was supported by the Russian Science Foundation, project no. 22-23-00750.

CONFLICT OF INTEREST

The authors declare that they have no conflicts of interest.

REFERENCES

1. Kovalenko, K.A., Potapov, A.S., and Fedin, V.P., *Russ. Chem. Rev.*, 2022, vol. 91, p. 5026. https://doi.org/10.1070/RCR5026
2. Agafonov, M.A., Aleksandrov, E.V., Artyukhova, N.A., et al., *Russ. J. Struct. Chem.*, 2022, vol. 63, no. 5, p. 671.
3. Monni, N., Oggianu, M., Sahadevan, S.A., et al., *Magnetochemistry*, 2021, vol. 7, p. 109.
4. Benmansour, S. and Gómez-García, C.J., *Magnetochemistry*, 2020, vol. 6, p. 71.
5. Liu, K.-G., Sharifzadeh, Z., Rouhani, F., et al., *Coord. Chem. Rev.*, 2021, vol. 436, p. 213827.
6. Wang, C. and Liao, K., *ACS Appl. Mater. Interfaces*, 2021, vol. 13, p. 56752.
7. Fasna, F. and Sasi, S., *ChemSelect*, 2021, vol. 6, p. 6365.
8. Antipin, I.S., Burilov, V.A., Gorbatchuk, V.V., et al., *Russ. Chem. Rev.*, 2021, vol. 90, p. 895. https://doi.org/10.1070/RCR5011
9. Kitagawa, S. and Matsuda, R., *Coord. Chem. Rev.*, 2007, vol. 251, p. 2490.
10. Kingsbury, C.J., Abrahams, B.F., Auckett, J.E., et al., *Chem.-Eur. J.*, 2019, vol. 25, p. 5222.
11. Abrahams, B.F., Dharma, A.D., Dyett, B., et al., *Dalton Trans.*, 2016, vol. 45, p. 1339.
12. Adil, K., Belmabkhout, Y., Pillai, R.S., et al., *Chem. Soc. Rev.*, 2017, vol. 46, p. 3402.
13. Ezugwu, C.I., Liu, S., Li, C., et al., *Coord. Chem. Rev.*, 2021, vol. 450, p. 214245.
14. Hu, Z. and Zhao, D., *CrystEngComm*, 2017, vol. 19, p. 4066.
15. Huangfu, M., Wang, M., Lin, C., et al., *Dalton Trans.*, 2021, vol. 50, p. 3429.
16. Li, P., Zhou, Z., Zhao, Y.S., et al., *Chem. Commun.*, 2021, vol. 57, p. 13678.
17. Wang, Y., Liu, X., Li, X., et al., *J. Am. Chem. Soc.*, 2019, vol. 141, p. 8030.
18. Chang, C.-H., Li, A.-C., Popovs, I., et al., *J. Mater. Chem. A*, 2019, vol. 7, p. 23770.
19. Calbo, J., Golomb, M.J., and Walsh, A., *J. Mater. Chem. A*, 2019, vol. 7, p. 16571.
20. Wang, M., Dong, R., and Feng, X., *Chem. Soc. Rev.*, 2021, vol. 50, p. 2764.
21. Dong, R. and Feng, X., *Nat. Mater.*, 2021, vol. 20, p. 122.
22. Benmansour, S. and Gómez-García, C.J., *Gen. Chem.*, 2020, vol. 6, p. 190033.
23. Espallargas, G.M. and Coronado, E., *Chem. Soc. Rev.*, 2018, vol. 47, p. 533.
24. Sahadevan, S.A., Manna, F., Abhervé, A., et al., *Inorg. Chem.*, 2021, vol. 60, p. 17765.
25. Trofimova, O., Maleeva, A.V., Ershova, I.V., et al., *Molecules*, 2021, vol. 26, p. 2486.
26. Sahadevan, S.A., Monni, N., Oggianu, M., et al., *ACS Appl. Nano Mater.*, 2020, vol. 3, p. 94.
27. Lysova, A.A., Kovalenko, K.A., Dybtsev, D.N., et al., *Microporous Mesoporous Mater.*, 2021, vol. 328, p. 111477.
28. Lysova, A.A., Samsonenko, D.G., Kovalenko, K.A., et al., *Angew. Chem., Int. Ed. Engl.*, 2020, vol. 59, p. 20561.
29. Lysova, A.A., Samsonenko, D.G., Dorovatovskii, P.V., et al., *J. Am. Chem. Soc.*, 2019, vol. 141, p. 17260.
30. Trofimova, O.Y., Maleeva, A.V., Arsenyeva, K.V., et al., *Crystals*, 2022, vol. 12, p. 370.
31. Trofimova, O.Y., Ershova, I.V., Maleeva, A.V., et al., *Russ. J. Coord. Chem.*, 2021, vol. 47, p. 610. https://doi.org/10.1134/S1070328421090086
32. Kharitonov, A.D., Trofimova, O.Y., Meshcheryakova, I.N., et al., *CrystEngComm*, 2020, vol. 22, p. 4675.
33. Khamaletdinova, N.M., Meshcheryakova, I.N., Piskunov, A.V., et al., *J. Struct. Chem.*, 2015, vol. 56, p. 233. https://doi.org/10.1134/S0022476615020055
34. *APEX3*, Madison: Bruker AXS Inc., 2018.
35. *Rigaku Oxford Diffraction. CrysAlisPro Software System. Version 1.171.38.46*, Wroclaw: Rigaku Corporation, 2015.
36. Krause, L., Herbst-Irmer, R., Sheldrick, G.M., et al., *J. Appl. Crystallogr.*, 2015, vol. 48, p. 3.
37. Sheldrick, G.M., *Acta Crystallogr., Sect. C: Struct. Chem.*, 2015, vol. 71, p. 3.
38. Sheldrick, G.M., *Acta Crystallogr., Sect. A: Cryst. Adv.*, 2015, vol. 71, p. 3.
39. Benmansour, S., Gómez-García, C.J., and Hernández-Paredes, A., *Crystals*, 2022, vol. 12, p. 261.
40. Benmansour, S., López-Martínez, G., Canet-Ferrer, J., et al., *Magnetochemistry*, 2016, vol. 2, p. 32.
41. Dubraja, L.A., Molcanov, K., Zilic, D., et al., *New J. Chem.*, 2017, vol. 41, p. 6785.
42. Vuković, V., Molčanov, K.I., Jelsch, C., et al., *Cryst. Growth Des.*, 2019, vol. 19, p. 2802.
43. Cao, H.-Y., Liu, Q.-Y., Gao, M.-J., et al., *Inorg. Chim. Acta*, 2014, vol. 414, p. 226.
44. Blatov, V.A., Shevchenko, A.P., and Proserpio, D.M., *Cryst. Growth Des.*, 2014, vol. 14, p. 3576.
45. Alexandrov, E.V., Blatov, V.A., Kochetkov, A.V., et al., *CrystEngComm*, 2011, vol. 13, p. 3947.
46. Aleksandrov, E.V., Shevchenko, A.P., Nekrasova, N.A., et al., *Russ. Chem. Rev.*, 2022, vol. 91, p. 5032. https://doi.org/10.1070/RCR5032
47. Alvarez, S., Alemany, P., Casanova, D., et al., *Coord. Chem. Rev.*, 2005, vol. 249, p. 1693.
48. Llunell, M., Casanova, D., Cirera, J., et al., *Universitat de Barcelona*, 2013.
49. Ruiz-Martinez, A., Casanova, D., and Alvarez, S., *Chem.-Eur. J.*, 2008, vol. 14, p. 1291.

Translated by E. Yablonskaya